Stationary and stable light-beam propagation in Kerr media with nonlinear absorption with controllable dissipation patterns

Miguel A. Porras,[1,*] Carlos Ruiz-Jiménez,[2] and Márcio Carvalho[2]

[1]*Grupo de Sistemas Complejos, Universidad Politécnica de Madrid, ETSIM, Rios Rosas 21, 28003 Madrid, Spain*
[2]*Grupo de Sistemas Complejos, Universidad Politécnica de Madrid, ETSIA, Ciudad Universitaria s/n, 28040 Madrid, Spain*

We report on the stationary and robust propagation of light beams with rather arbitrary and controllable intensity and dissipation transverse patterns in self-focusing Kerr media with nonlinear absorption. When nonlinear absorption is due to multiphoton ionization at high beam powers in transparent media such as glasses and air, these beams can generate multiple plasma channels with tailored geometries. Their nature and spatial characteristics are discussed in detail, as well as the laws determining their spontaneous formation from coherent superpositions of Bessel beams of different amplitudes and topological charges.

I. INTRODUCTION

The achievement of localized, stationary, and stable propagation of multidimensional waves in homogeneous, isotropic nonlinear media is one of the main problems in nonlinear optics and constitutes a broad area of research today [1–3]. Many of the elaborated solutions, some of them realized experimentally, rely on two broad models. The first one is the conservative model based on nonlinear Schrödinger equations with dispersive, Kerr-type nonlinearities and others, describing passive propagation of intense waves in unbounded transparent media. The second model is the complex Ginzburg-Landau equation in systems with gain and loss, as laser cavities [4–6]. More or less broad families of solitons and dissipative solitons (also called autosolitons or cavity solitons) with a variety of geometries have been reported to be supported by these models. Given their relation to the present article, we mention the families of vortex solitons—solitons with a nested vortex [7], their azimuthally modulated versions called azimuthons [8,9], and solitons clusters [10] (see [11] for a review). In conservative models, a stable balance between diffraction and the dispersive nonlinearities supports robust stationary propagation. In the dissipative model, an additional balance is needed between gain and losses [12–14].

Nonconservative models involving only losses are usually left aside because they do not support solitons, in the sense of self-trapped structures. However, the nonlinear Schrödinger equation with purely loss terms and no gain terms arises naturally in situations as common as light-beam propagation in transparent dielectrics media at intensities such that multiphoton absorption processes are relevant. The existence of light beams, called nonlinear unbalanced Bessel beams, with the ability to propagate without any change, including no attenuation, in media with Kerr-type nonlinearities and nonlinear absorption, was described in 2004 [15]. They provided a theoretical basis for interpreting some features of light filaments generated from intense, ultrashort pulses [16–18], where nonlinear absorption arises from multiphoton ionization, particularly the replenishment and self-healing

mechanisms involved in their robust and quasistationary propagation [19–25]. Stationarity with nonlinear absorption is indeed possible for waves less strongly localized than solitons, as nonlinear versions of Bessel-like and Airy-like beams [26,27] carrying, ideally, an infinite amount of power or a power reservoir. In these beams [15,28–31] the power in the reservoir is permanently flowing towards the central region of high intensity, where most nonlinear power losses take place, replenishing it. After the fundamental nonlinear unbalanced Bessel beam [15], the same mechanism has more recently been shown to work with high-order (vortex-carrying) nonlinear Bessel beams [28–30]. Here we refer to all of them as nonlinear Bessel vortex beams (BVBs), the fundamental beam being the particular vortexless situation.

Nonlinear BVBs have proven to be particularly fruitful for explaining the filamentation dynamics seeded by ultrashort (linear) Bessel beams [29,30,32–39]. Even if the physics of filamentation involves complex light-matter interactions and rich spatiotemporal dynamics [16–18], the three key phenomena determining substantially the filamentation dynamics with conical beams are just those supporting the stationarity of nonlinear BVBs, namely, diffraction, Kerr self-focusing, and nonlinear absorption [29,30,32]. The steady and unsteady regimes of filamentation observed in the filamentation with the lowest order Bessel beam [32] have been successfully explained in terms of nonlinear BVB attractors and their stability properties [40]. More recently, tubular filamentation from vortex-carrying Bessel beams has been created [29,30] and has also been interpreted as the formation of a vortex-carrying nonlinear BVB that is stable against radial and azimuthal perturbations [41]. The disintegration of the tubular regime into rotary or random filaments observed in related experiments is also explained in terms of the development of the azimuthal instability of unstable nonlinear BVBs [41].

The intensity profiles of nonlinear BVBs are all circularly symmetric, and so are the dissipation channels that they can generate. The tubular regime is a sophisticated example of a "tailored" or controlled transversal pattern, which is expected to open new perspectives in laser-powered material processing and other applications [30,42–46]. Complex filamentation patterns other than circular arise naturally in multiple filamentation from small-scale self-focusing of laser beams carrying

---

*miguelangel.porras@upm.es

many critical powers [16–18] or from the azimuthal instability of tubular filaments [29,30,41], but originating from noisy perturbations, these patterns are largely uncontrollable and far from being propagation invariant.

In this paper we investigate whether propagation-invariant light beams with other geometries, preferably with controllable intensity and dissipation patterns, are supported by transparent dielectrics with self-focusing nonlinearities and nonlinear absorption. We find an affirmative answer when studying by means of numerical simulations the nonlinear propagation dynamics seeded by illuminating the medium with coherent superpositions of Bessel beams of different topological charges and amplitudes. These (linear) Bessel-beam superpositions are easily generated using spatial light modulators [47–49], illuminating an axicon with several coherent Gaussian beams with embedded vorticities or with superpositions of Laguerre-Gauss beams [50]. For a range of the parameters that define the input Bessel-beam superposition and the material medium, stationary and stable propagation states constantly dissipating their power along organized and narrow channels are seen to emerge spontaneously. We confine ourselves to the superposition of two Bessel beams, where the channel geometry is primarily controlled by their amplitudes and topological charges, and the variety of intensity and dissipation patterns is already very vast.

To clearly distinguish these states from other known localized structures, first we present the more general states without any particular symmetry, and then we focus on those with n-fold rotational symmetry formed from superpositions of two Bessel beams of opposite topological charges, resembling azimuthons [8,9,12–14]. These structures are nevertheless neither conservative nor supported by a gain-loss balance, and they do not rotate either. Given the distinctive properties of having arbitrary shapes and of not being supported by gain, i.e., of being strictly dissipative, we have called them *dissipatons*.

Outside their central region, dissipatons are always seen to have linear conical tails, and therefore a power reservoir, shaped like a superposition of unbalanced Bessel beams (i.e., with unequal inward and outward Hänkel-beam amplitudes), all of them with the same cone angle but different topological charges. The excess of the inward Hänkel-beam amplitudes creates an inward radial current, like that in nonlinear BVBs but with an azimuthal dependence, and such that the net power flux coming from the reservoir equals the total power loss rate in the dissipative core. We find simple rules that describe the dissipaton formation. Given an input superposition of Bessel beams, the dissipaton that emerges preserves the cone angle, the topological charges, and the amplitudes of the inward Hänkel components of all input Bessel beams. Although the dissipative center has a more complex structure of intertwined hot spots and vortices, it reflects to a certain extent the structure of the linear tails, and therefore that of the input Bessel-beam superposition, the dissipation pattern then being quite controllable. Numerical simulations also show that dissipatons are stable under large perturbations strongly distorting the dissipative center. In fact, the only condition for the whole dissipaton structure to emerge spontaneously is the presence of inward currents carried by its inward Hänkel-beam components.

II. BASIC RELATIONS

According to the above, we consider the propagation of a paraxial light beam $E = \text{Re}\{A \exp[i(kz - \omega t)]\}$, with carrier frequency ω, propagation constant $k = n\omega/c$ (n is the linear refractive index and c the speed of light in vacuum), and complex envelope A. We assume that cubic Kerr nonlinearity and nonlinear absorption are the dominating nonlinearities of the medium. As with nonlinear BVBs, other dispersive nonlinearities (quintic, saturable) could be considered as well without substantial changes in the results. The evolution of the envelope is then ruled by the nonlinear Schrödinger equation

$$\partial_z A = \frac{i}{2k}\Delta_\perp A + i\frac{kn_2}{n}|A|^2 A - \frac{\beta^{(M)}}{2}|A|^{2M-2}A, \quad (1)$$

where $\Delta_\perp$ is the transverse Laplacian given by $\Delta_\perp = \partial_r^2 + (1/r)\partial_r + (1/r^2)\partial_\varphi^2$ in cylindrical coordinates (r,φ,z), $n_2 > 0$ is the nonlinear refractive index, and $\beta^{(M)} > 0$ is the M-photon absorption coefficient.

At low enough intensities (neglecting the nonlinear terms), Eq. (1) is satisfied by the linear (and paraxial) Bessel beams $A(r,\varphi,z) \propto J_s(k\theta r)e^{is\varphi}e^{i\delta z}$ of cone angle θ, with an axial wave vector shortened by $\delta = -k\theta^2/2 < 0$, and carrying a vortex of topological charge s. To investigate nonlinear beams characterized also by a cone angle θ but at high intensities, we find it convenient to use the scaled and dimensionless radial coordinate, propagation distance, and envelope,

$$\rho \equiv k\theta r = \sqrt{2k|\delta|}r, \quad \zeta \equiv |\delta|z, \quad \tilde{A} \equiv \left(\frac{\beta^{(M)}}{2|\delta|}\right)^{\frac{1}{2M-2}}A \quad (2)$$

[in many of the figures, we also use the dimensionless Cartesian coordinates $(\xi,\eta) \equiv (k\theta x, k\theta y)$], to rewrite Eq. (1) as

$$\partial_\zeta \tilde{A} = i\Delta_\perp \tilde{A} + i\alpha|\tilde{A}|^2\tilde{A} - |\tilde{A}|^{2M-2}\tilde{A}, \quad (3)$$

where now $\Delta_\perp = \partial_\rho^2 + (1/\rho)\partial_\rho + (1/\rho^2)\partial_\varphi^2$ is the transverse Laplacian in the dimensionless coordinates, and

$$\alpha \equiv \left(\frac{2|\delta|}{\beta^{(M)}}\right)^{1/(M-1)}\frac{kn_2}{n|\delta|}. \quad (4)$$

With these variables, the linear Bessel beams reads $\tilde{A} \propto J_s(\rho)e^{is\varphi}e^{-i\zeta}$. Values of $|\tilde{A}|^2$ of the order of unity correspond to the typical values of the intensities involved in filamentation experiments in solids or gases, e.g., at 800 nm with cone angle $\theta = 1°$ in water ($n = 1.33$, $n_2 = 2.6 \times 10^{-16}$ cm^2/W, $M = 5$, and $\beta^{(5)} = 8.3 \times 10^{-50}$ cm^7/W^4 [51]) or $\theta = 0.1°$ in air ($n \simeq 1$, $n_2 = 3.2 \times 10^{-19}$ cm^2/W, $M = 8$, and $\beta^{(8)} = 1.8 \times 10^{-94}$ cm^{13}/W^7 [51]); $|\tilde{A}|^2 \simeq 1$ corresponds to 4 and 20 TW/cm^2, respectively. The value of the parameter α is determined by the cone angle and the medium properties at the light wavelength. At 800 nm in water, the values of α range from 0.17 to 5.3 for cone angles θ from $10°$ to $1°$; in air, α varies between 0.08 and 4.2 for θ varying between $1°$ and $0.1°$.

We further write the complex envelope as $\tilde{A} = \tilde{a}e^{i\Phi}$, where $\tilde{a} > 0$ and Φ are its real amplitude and phase. The nonlinear

Schrödinger equation, (3), is then seen to be equivalent to the energy transport and eikonal equations

$$\tfrac{1}{2}\partial_\zeta \tilde{a}^2 + \nabla_\perp \cdot \mathbf{j} = -\tilde{a}^{2M},\tag{5}$$

$$\partial_\zeta \Phi = \frac{\Delta_\perp \tilde{a}}{\tilde{a}} - |\nabla_\perp \Phi|^2 + \alpha \tilde{a}^2,\tag{6}$$

where $\nabla_\perp = \mathbf{u}_\rho \partial_\rho + \mathbf{u}_\varphi (1/\rho)\partial_\varphi$, $\mathbf{u}_\rho$ and $\mathbf{u}_\varphi$ are unit radial and azimuthal vectors, and $\mathbf{j} = \tilde{a}^2 \nabla_\perp \Phi = \mathrm{Im}\{\tilde{A}^\star \nabla_\perp \tilde{A}\}$ is the current of the intensity $\tilde{a}^2$ in the transversal plane. Nonlinear BVBs were described as particular solutions to Eq. (5) and Eq. (6) that generalize Bessel beams to nonlinear media, whose intensity profiles are propagation invariant and circularly symmetric [15,28–30]. Here we search for conical beams of the most general form, $\tilde{A} = \tilde{a}(\rho,\varphi)e^{i\phi(\rho,\varphi)}e^{-i\zeta}$, whose intensity profiles $\tilde{a}^2(\rho,\varphi)$ are also localized but may not have any particular symmetry. According to Eqs. (5) and (6), their amplitude and phase patterns, $a(\rho,\varphi)$ and $\phi(\rho,\varphi)$, must satisfy

$$\nabla_\perp \cdot \mathbf{j} = -\tilde{a}^{2M},\tag{7}$$

$$\Delta_\perp \tilde{a} - |\nabla_\perp \phi|^2 \tilde{a} + \tilde{a} + \alpha \tilde{a}^3 = 0,\tag{8}$$

where $\mathbf{j} = \tilde{a}^2 \nabla_\perp \phi$ is the ζ-independent intensity current. Equation (7) expresses the general condition for a conical beam to propagate without any change in a medium with absorption. Integrating over an arbitrary area S in the transversal plane and using the divergence theorem, this condition is readily seen to be equivalent to

$$-\oint_C \mathbf{j} \cdot \mathbf{n}\, dl = \int_S \tilde{a}^{2M} ds,\tag{9}$$

or $-F_C = N_S$ for short, where dl is a differential element of the contour C of S, $\mathbf{n}$ is the outward normal unit vector, and ds an elemental area of S. This condition thus establishes that the power loss rate N_S in any region S of the transversal plane is offset by an inward power flux $-F_C$ though its contour for stationary propagation to be possible. In particular, applying Eq. (9) to a circle of large enough radius ρ for the total nonlinear power losses to occur inside it (assuming that they are finite), this condition requires

$$F_\infty \equiv -\int_0^{2\pi} j_\rho(\rho,\varphi)\rho\, d\varphi = N_\infty \tag{10}$$

for $\rho \to \infty$, i.e., an inward power flux from the power reservoir of the conical beam that is independent of the large radius ρ and that replenishes the power losses,

$$N_\infty \equiv \int_{\mathbb{R}^2} \tilde{a}^{2M} ds,\tag{11}$$

in the entire transversal section.

A direct search of solutions of the nonlinear partial differential equations, (7) and (8), without simplifying assumptions, such as circular symmetry, separability of the intensity and phase patterns in ρ and φ, and particular boundary conditions, is complicated. An alternate procedure is suggested by a well-established connection between linear Bessel beams and nonlinear BVBs in the circularly symmetric case, as summarized below.

III. CIRCULARLY SYMMETRIC CASE: NONLINEAR BESSEL VORTEX BEAMS

If a powerful Bessel beam is introduced into the medium, its nonlinear dynamics is determined by the existence and properties of an attracting nonlinear BVB [40,41]. Given the input Bessel beam $\tilde{A}(\rho,\varphi,\zeta = 0) = b_L J_s(\rho)e^{is\varphi}$, or equivalently $\tilde{A}(\rho,\varphi,\zeta = 0) = \tfrac{1}{2}[b_L H_s^{(1)}(\rho) + b_L H_s^{(2)}(\rho)]e^{is\varphi}$, the attracting nonlinear BVB, $\tilde{a}(\rho)e^{i\phi(\rho)}e^{is\varphi}e^{-i\zeta}$, has the same cone angle and topological charge as the linear Bessel beam and behaves asymptotically at a large radius ρ, where it remains linear, as the unbalanced Bessel beam $\tilde{A} \simeq \tfrac{1}{2}[b_{\mathrm{out}} H_s^{(1)}(\rho) + b_{\mathrm{in}} H_s^{(2)}(\rho)]e^{is\varphi}e^{-i\zeta}$, with the property that $|b_{\mathrm{in}}| = b_L$ [28,40,41]. The conservation of the cone angle, the topological charge, and the amplitude of the inward Hänkel-beam component specifies unambiguously an attracting nonlinear BVB for any input Bessel beam. Using the equivalent expressions

$$H_s^{(1,2)}(\rho) \simeq \sqrt{\frac{2}{\pi\rho}} e^{\pm i(\rho - \pi/4 - \pi s/2)},\tag{12}$$

of the Hänkel functions at large ρ, the outward Hänkel beam, $(b_{\mathrm{out}}/2)H_s^{(1)}(\rho)e^{is\varphi}e^{-i\zeta}$, is seen to carry the current $\mathbf{j} = (|b_{\mathrm{out}}|^2/2\pi\rho)[\mathbf{u}_\rho + (s/\rho)\mathbf{u}_\varphi]$ spirally outwards, while the inward Hänkel beam, $b_{\mathrm{in}} H_s^{(2)}(\rho)e^{is\varphi}e^{-i\zeta}$, carries the current $\mathbf{j} = (|b_{\mathrm{in}}|^2/2\pi\rho)[-\mathbf{u}_\rho + (s/\rho)\mathbf{u}_\varphi]$ spirally inwards. From the asymptotic form of nonlinear BVBs and Eq. (10), one then gets the relation $-F_\infty = |b_{\mathrm{in}}|^2 - |b_{\mathrm{out}}|^2 = N_\infty$ for the inward power flux restoring the total power losses in the nonlinear BVB.

The particular Bessel-beam dynamics depends on the stability properties of the attracting nonlinear BVB. According to the linear-stability analysis in Refs. [40] and [41], there exist nonlinear BVBs that are stable against radial and azimuthal perturbations. In the case of stability, the Bessel-beam dynamics ends in the complete formation of the nonlinear BVB. The example in Fig. 1 summarizes these previous results. The input Bessel beam represented by the light-gray curve in Fig. 1(a) transforms into the nonlinear BVB represented by the black curve, having a radial inward component of the intensity current that sustains the stationarity, as shown in Fig. 1(b). After a transient, the peak intensity and nonlinear power losses N_∞ reach constant values corresponding to the attracting nonlinear BVB [light-gray curves in Fig. 1(c)].

The fact that the linearly stable nonlinear BVB is formed starting from so distant an initial condition as the linear Bessel suggests stability under large perturbations within a certain attraction basin. Additional numerical simulations indicate that the same final nonlinear BVB is formed when the input beam carries at large radius only the inward Hänkel-beam component that is preserved in the propagation. The attraction basin of the nonlinear BVB then includes all beams of the type $\tilde{A} = \tfrac{1}{2}b_L H_s^{(2)}(\rho)e^{is\varphi} + f(\rho,\varphi)$, where $f(\rho,\varphi)$ does not carry any additional inward radial current at large radius. The dark-gray curves in Figs. 1(a) and 1(c) show the radial intensity profile of an input beam with these characteristics that transforms into the same nonlinear BVB, and the peak intensity and power losses reach the same constant values as with the input Bessel beam.
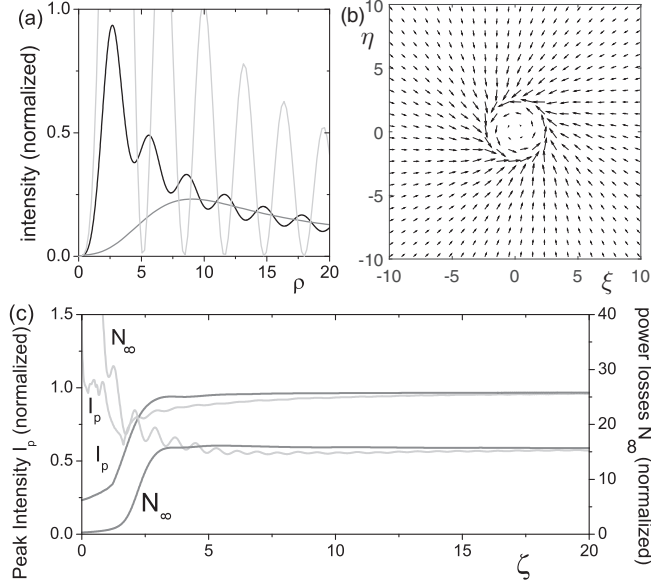
FIG. 1. (a) Intensity of the initial Bessel beam, $\tilde{A}(\rho,\varphi,\zeta=0) = b_L J_s(\rho)e^{is\varphi}$, $b_L = 4$, $s = 2$ (light-gray curve), of the initial "holed" Hänkel beam, $\tilde{A}(\rho,\varphi,\zeta=0) = \frac{1}{2}b_L H_s^{(2)}(\rho)e^{is\varphi}(1 - e^{-\rho^2/\rho_0^2})$, $b_L = 4$, $s = 2$, hole radius $\rho_0 = 6$, with the same asymptotic inward intensity current (dark-gray curve), and the stationary intensity profile of the attracting nonlinear BVB formed at $\zeta = 20$ (black curve) in a medium and with a cone angle such that $M = 5$ and $\alpha = 0.5$. (b) Intensity current in the transversal plane of the attracting nonlinear BVB. (c) Peak intensity and nonlinear power losses versus propagation distance for the input Bessel beam (light-gray curves) and for the holed Hänkel beam (dark-gray curves). All quantities are normalized as explained in the text. Normalized Cartesian coordinates are $(\xi,\eta) = (k\theta x, k\theta y)$.

IV. DISSIPATONS

With the above in mind, we investigate the beam propagation dynamics that results from illuminating the medium with the coherent superposition $\tilde{A}(\rho,\varphi,\zeta=0) = \sum_j b_{L,j} J_{s_j}(\rho)e^{is_j\varphi}$ of several Bessel beams with the same cone angle but different topological charges s_j and amplitudes $b_{L,j}$. A large variety of input-beam profiles can be obtained with different choices of the parameters of these superpositions, which are easily generated in laboratories [47–49]. In this section we consider the most general situation where this input beam does not have any particular symmetry in its transversal sections. As above, we will also consider illuminating the medium with other beams carrying the same inward intensity
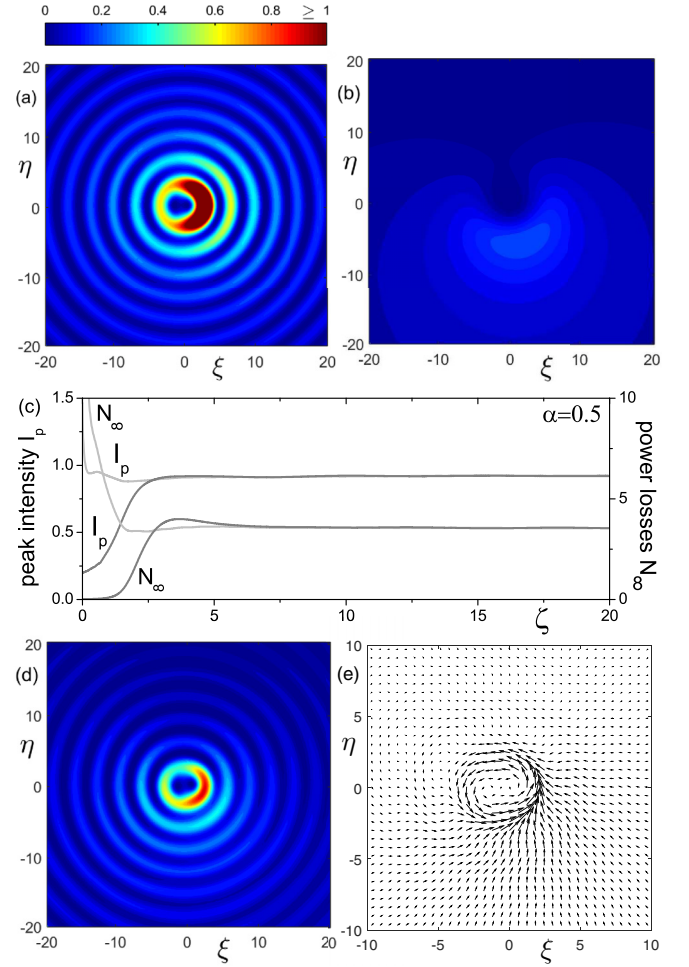

FIG. 2. Intensity of the input superposition of (a) two Bessel beams, with $s_1 = 2$, $b_{L,1} = 2$ and $s_2 = 1$, $b_{L,2} = 1$, and (b) two inward Hänkel beams with the same parameters multiplied by $(1 - e^{-\rho^2/\rho_0^2})$, $\rho_0 = 4$, to eliminate the Hänkel singularities at the origin without modifying the inward current at a large radius. (c) In a medium and for a cone angle such that $M = 5$ and $\alpha = 0.5$, normalized peak intensity and nonlinear power losses versus propagation distance for the input Bessel superposition (light-gray curves) and for the input Hänkel superposition (dark-gray curves). (d, e) The propagation-invariant intensity and current patterns at a large propagation distance ($\zeta = 30$). All quantities are dimensionless, as explained in the text. Dimensionless Cartesian coordinates are $(\xi,\eta) = (k\theta x, k\theta y)$.

currents, as $\tilde{A}(\rho,\varphi,\zeta=0) = \sum_j \frac{1}{2}b_{L,j} H_{s_j}^{(2)}(\rho)e^{is_j\varphi} + f(\rho,\varphi)$ at large radius.

In Fig. 2 we have chosen two superposed beams with $s_1 = 2$, $b_{L,1} = 2$ and $s_2 = 1$, $b_{L,2} = 1$ in a medium and with cone angle such that $M = 5$ and $\alpha = 0.5$. The intensity patterns of the input Bessel-beam superposition [Fig. 2(a)] and of the input Hänkel-beam superposition [Fig. 2(b)] differ substantially; so also does their propagation in the medium. The input Bessel superposition is strongly absorbed at first, while the input Hänkel superposition builds up [Fig. 2(c)]. Regardless of whether the Bessel superposition or the Hänkel superposition is launched, the peak intensity and total power losses reach the same positive constant values at long distances. These values correspond to the same final, nonlinear stationary

On the opposite side, if the attracting nonlinear BVB determined by the conservation of the cone angle, the topological charge, and the amplitude of the inward Hänkel-beam component turns out to be unstable (according to the linear-stability analysis), the Bessel-beam dynamics consists in the growth of its unstable modes, developing into large, periodic or chaotic oscillations around the nonlinear BVB if radial instability is dominant [40] or leading to circular symmetry breaking and a complex dynamics of rotatory or random spots if azimuthal instabilities dominate [41].

state that attracts the two beams, whose intensity and intensity current patterns in a transversal plane are shown in Figs. 2(d) and 2(e).

These numerical simulations, and others below, show that the Kerr medium with nonlinear losses supports stationary propagation of beams that do not have any specific symmetry, to which we refer as "dissipatons." In the example in Fig. 2, the final state has even lost the bilateral symmetry of the input beam. The two vortices of unit charge in the final state are slightly displaced in the dissipaton from those in the input Bessel-beam superposition.

In Figs. 3(a)–3(d) we have plotted the peak intensity and nonlinear power losses as functions of the propagation distance for the same couple of input Bessel and Hänkel superpositions as above but several increasing values of α (e.g., increasing n_2 or diminishing cone angle). Above a certain threshold, say α_{max} ($\alpha_{max} \simeq 1.5$ in this example), which depends on the particular input superposition and M, the dynamics does not lead to a stationary propagation regime, regardless of whether Bessel or Hänkel superpositions are introduced in the medium. The propagation-invariant intensity profiles of the dissipatons from $\alpha \simeq 0$ (large enough cone angle or negligible Kerr nonlinearity) and to the maximum value $\alpha_{max} \simeq 1.5$ [Figs. 3(e) and 3(f)] feature increasing compression and irregularity of the nonlinear core.

Similar results are seen to hold for other input beams. In the example in Fig. 4 we wanted to produce a triangular dissipaton with a fourth hot spot at its center. For this we chose Bessel or Hänkel superpositions with topological charges $s_1 = 3$ and $s_2 = 0$. All intensity patterns in Fig. 4 correspond to the same cone angle and the same medium ($\alpha = 0.5$ and $M = 5$) but increasing intensities ($b_{L,1} = b_{L,2} \equiv b_L = 0.5, 1.5$, and 3). As above, these patterns become increasingly irregular, and no stationary state is reached above a certain value of b_L that depends on the values of other parameters (above $b_L = 3$ in this example). Figure 4 also shows the respective current patterns **j** and their associated sinks equal to the dissipation patterns $|\tilde{A}|^{2M}$. An input power such that $b_L = 1.5$ produces four approximately equal dissipative spots. These examples, and others considered in Sec. V, illustrate that dissipation occurs only in strongly localized spots, and not in the outer rings of the intensity pattern, and that these dissipative spots can be organized almost arbitrarily with an adequate choice of the topological charges and intensities of the input-beam superposition.

Asymptotic structure of dissipatons

The structure of the nondissipative outer part of dissipatons is found to be simpler than that of the dissipative spots. At fixed azimuthal angle φ and increasing radius the intensity is always seen to decay as ρ^{-1} while oscillating harmonically. The same happens with the circularly symmetric nonlinear BVBs [15,28], but now the decay rate and the oscillation contrast depend on the specific azimuthal angle. This leads us to conjecture a linear conical structure for these tails of the form

$$\tilde{A} \simeq \sum_j \frac{1}{2}\left[b_{\text{out},j} H_{s_j}^{(1)}(\rho) + b_{\text{in},j} H_{s_j}^{(2)}(\rho)\right] e^{is_j\varphi} e^{-i\zeta}, \quad (13)$$
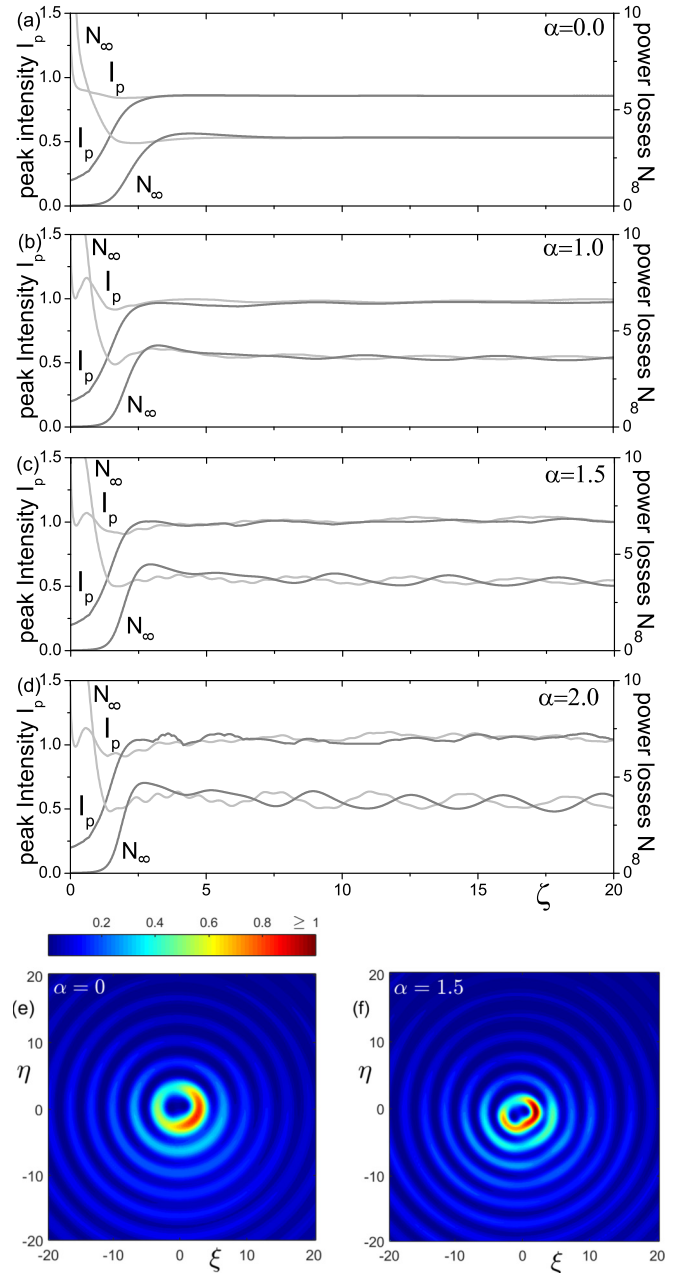

FIG. 3. (a–d) For the same input Bessel and Hänkel superpositions as in Fig. 2, peak intensity and nonlinear power losses versus propagation distance for $M = 5$ and increasing values of α. For the larger values of α these quantities do not reach constant values, indicating that a propagation-invariant state is not formed. (e, f) Intensity profiles of the final propagation-invariant states for $\alpha \simeq 0.0$ and the maximum value $\alpha = \alpha_{max} \simeq 1.5$ leading to the formation of a propagation-invariant beam. Their intensity profiles are increasingly compressed with increasing strength of the Kerr nonlinearity.

i.e., a linear superposition of unbalanced Bessel beams. Using Eq. (12) for Hänkel beams at a large radius, Eq. (13) can also be written as

$$\tilde{A} \simeq \frac{1}{\sqrt{2\pi\rho}}\left[b_{\text{out}}(\varphi)e^{i(\rho-\pi/4)} + b_{\text{in}}(\varphi)e^{-i(\rho-\pi/4)}\right]e^{-i\zeta}, \quad (14)$$
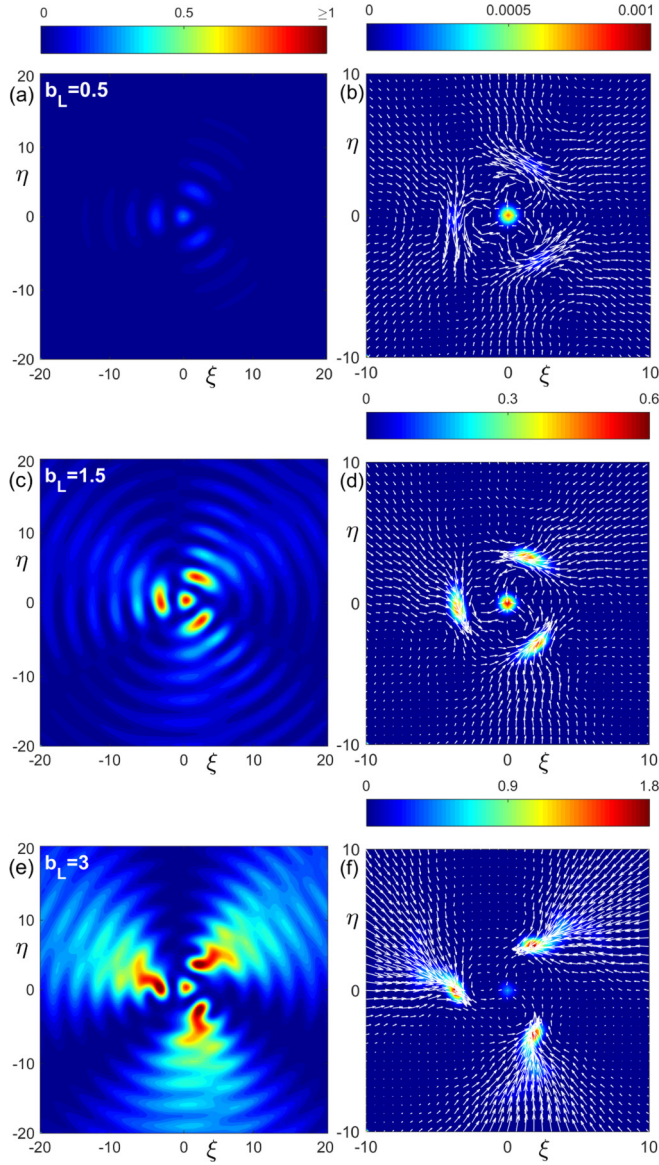
FIG. 4. (a, c, e) Intensity patterns $|\tilde{A}|^2$ and (b, d, f) corresponding dissipation $|\tilde{A}|^{2M}$ and intensity current $\mathbf{j}$ patterns of the dissipatons formed with cone angles and media such that $\alpha = 0.5$ and $M = 5$ starting from two conical beam superpositions, with $s_1 = 3$ and $s_2 = 0$, and increasing amplitudes, $b_{L,1} = b_{L,2} = b_L = 0.5$, 1.5, and 3.

where we have defined

$$b_{\text{out}}(\varphi) \equiv \sum_j b_{\text{out},j} e^{is_j(\varphi - \pi/2)}, \qquad (15)$$

$$b_{\text{in}}(\varphi) \equiv \sum_j b_{\text{in},j} e^{is_j(\varphi + \pi/2)}. \qquad (16)$$

Equation (14) then yields an intensity profile at a large radius given by

$$2\pi\rho|\tilde{A}|^2 \simeq |b_{\text{out}}(\varphi)|^2 + |b_{\text{in}}(\varphi)|^2 + 2|b_{\text{out}}(\varphi)||b_{\text{in}}(\varphi)|$$
$$\times \cos[2(\rho - \pi/4) + \kappa(\varphi)], \qquad (17)$$

where $\kappa(\varphi) = \arg b_{\text{out}}(\varphi) - \arg b_{\text{in}}(\varphi)$. As a function of ρ, Eq. (17) represents harmonic oscillations of φ-dependent

contrast,

$$C(\varphi) = \frac{2|b_{\text{out}}(\varphi)||b_{\text{in}}(\varphi)|}{|b_{\text{out}}(\varphi)|^2 + |b_{\text{in}}(\varphi)|^2}, \qquad (18)$$

about the φ-dependent mean value

$$R(\varphi) = |b_{\text{out}}(\varphi)|^2 + |b_{\text{in}}(\varphi)|^2. \qquad (19)$$

The linearity of these tails allows us to generalize the result in the circularly symmetric case [28] where the cone angle and all topological charges s_j and amplitudes of the inward Hänkel beams in the asymptotic expression, (13), of a dissipaton are the same as those of the input beam; i.e.,

$$|b_{\text{in},j}| = |b_{L,j}| \quad \text{for all } j. \qquad (20)$$

Also, the asymptotic expression for the radial component of the intensity current can be evaluated to be $j_\rho \simeq \text{Im}\{\tilde{A}^\star \partial_\rho \tilde{A}\} = [|b_{\text{out}}(\varphi)|^2 - |b_{\text{in}}(\varphi)|^2]/(2\pi\rho)$. From Eq. (10), we obtain a constant inward radial flux at a large radius offsetting the total power losses as

$$-F_\infty = -\int_0^{2\pi} \frac{|b_{\text{out}}(\varphi)|^2 - |b_{\text{in}}(\varphi)|^2}{2\pi} d\varphi = N_\infty, \qquad (21)$$

and upon integration, the relation

$$\sum_j |b_{\text{in},j}|^2 - \sum_j |b_{\text{out},j}|^2 = N_\infty \qquad (22)$$

between the amplitude of the inward and that of the outward Hänkel-beam components.

The validity of all previous relations is supported by the numerical analysis. As an example, Figs. 5(a) and 5(b) show the intensity profile of a dissipaton [the same as in Figs. 3(a) and 3(e)] and the fitted intensity profile (for $\rho > 5$) using Eq. (13) with $b_{\text{in},j}$ and $b_{\text{out},j}$ satisfying Eqs. (20) and (22) (see caption for detailed values). The radial profiles of the dissipaton and of the asymptotic form at two particular azimuthal angles are more clearly shown to match better and better with increasing radius in Fig. 5(c). With the values of $b_{\text{in},j}$ and $b_{\text{out},j}$, one can evaluate $b_{\text{in}}(\varphi)$ and $b_{\text{out}}(\varphi)$ from Eqs. (15) and the contrast $C(\varphi)$ and average oscillation value $R(\varphi)$ of the radial oscillations at each azimuthal direction from Eqs. (18) and (19). These are plotted in Figs. 5(d) and 5(e) in the above example. Compared to the same quantities for the input Bessel-beam superposition (dashed curves), the average value of the oscillations is significantly smaller due to the initial stage of strong absorption. It is also characteristic of dissipatons that the contrast of the oscillations is significantly diminished along the azimuthal directions of high intensity, i.e., high $R(\varphi)$, as for the angle $\varphi = 3\pi/2$ in this example.

Additional confirmation of the generality of the above description is given in Sec. V for dissipatons with n-fold rotational symmetry. By analogy with nonlinear BVBs, each dissipaton is determined by the set of parameters M, α, s_j, and $b_{L,j}$. We can conjecture, following the same analogy, that there exist dissipatons with any value of these parameters, as for nonlinear BVBs [28], and that they may be stable or unstable for different choices of the parameters, e.g., unstable above $\alpha_{\max}$ once the other parameters are fixed. This hypothesis is suggested by the fact that when the propagation does not lead to a stationary state, as in Fig. 3(d), the beam is not completely
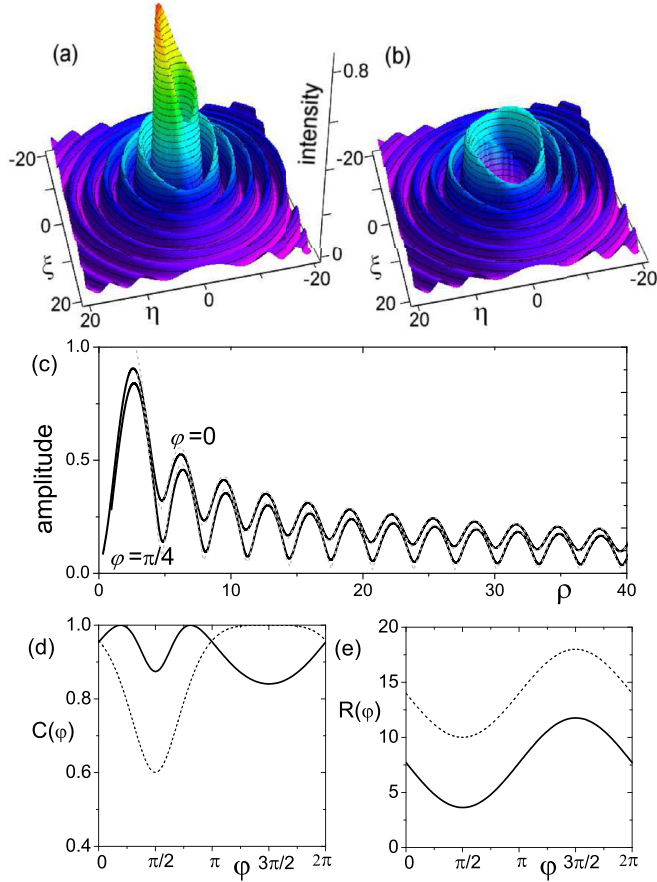
FIG. 5. (a) Intensity distribution of the dissipaton formed in media with $M = 5$ and $\alpha \simeq 0$ starting with the Bessel-beam superposition with $s_1 = 2$, $b_{L,1} = 2$ and $s_2 = 1$, $b_{L,2} = 1$. (b) Intensity distribution (for $\rho > 5$) of the asymptotic form in Eq. (13) with $b_{\text{in},1} = b_{L,1} = 2$, $b_{\text{in},2} = b_{L,2} = 1$, $b_{\text{out},1} \simeq 1.11$, and $b_{\text{out},2} = 0.64\,e^{i0.70}$, verifying that $|b_{\text{in},1}|^2 + |b_{\text{in},2}|^2 - |b_{\text{out},1}|^2 - |b_{\text{out},2}|^2 = N_\infty = 3.35$ [see Fig. 3(e)]. (c) Radial amplitude distributions (solid black curves) and their asymptotic fitting with the above values (dashed gray curves) for the azimuthal angles $\varphi = 0$ and $\varphi = \pi/4$, featuring decaying oscillations of different contrasts about different mean values. The amplitude instead of the intensity is shown for clarity. (d, e) Contrast and average value of the radial oscillations in each azimuthal direction obtained from the above values of the Hänkel-beam amplitudes and Eqs. (18) and (19). Dashed curves are the same quantities for the input Bessel-beam superposition.

dissipated or dispersed, but its peak intensity, its power losses, and the entire beam profile oscillate more or less randomly about constant values, as in the circularly symmetric case [41].

V. DISSIPATONS WITH $2s$-FOLD ROTATIONAL SYMMETRY

Of particular interest are the dissipatons with $2s$-fold rotational symmetry formed from two Bessel beams,

$$\tilde{A}(\rho,\varphi,0) = b_{L,s}J_s(\rho)e^{is\varphi} + b_{L,-s}J_{-s}(\rho)e^{-is\varphi}, \qquad (23)$$

of opposite topological charges $\pm s$. Without loss of generality, we can choose real and positive $b_{L,s}$ and $b_{L,-s}$, since the only effect of a phase shift between them is a rigid-beam rotation.
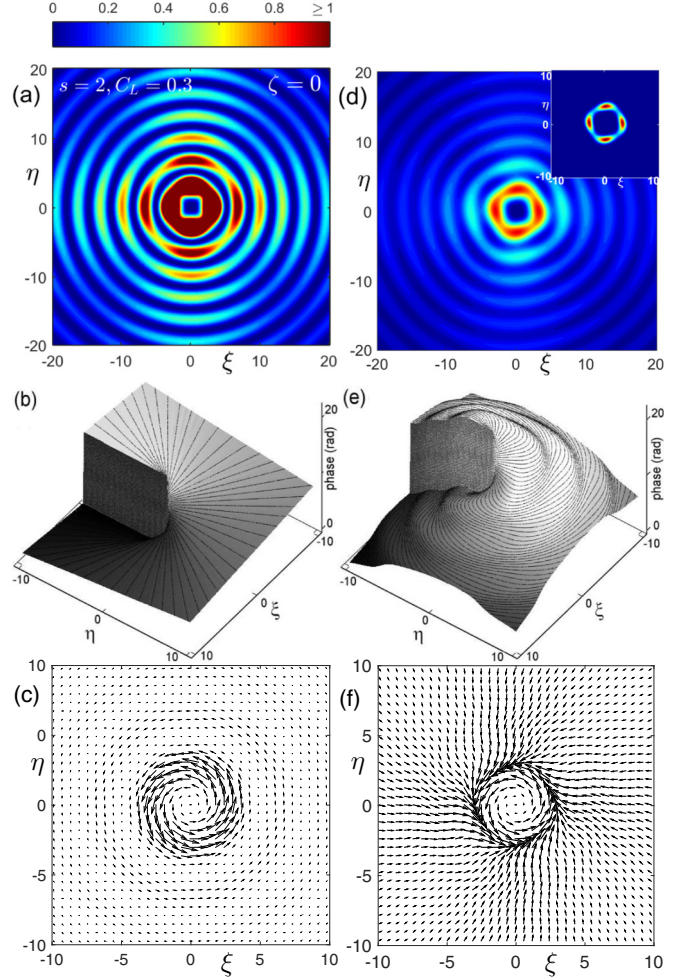

FIG. 6. (a) Intensity, (b) phase, and (c) intensity current of the initial superposition of two Bessel beams of opposite charges, $s = 2$ and $-s = -2$, average amplitude $b_L = 3$, and azimuthal contrast $C_L = 0.3$ ($b_{L,s} = 2.965$ and $b_{L,-s} = 0.455$). (d) Intensity, (e) phase, and (f) intensity current of the final stationary state in the form of a dissipaton formed in a medium with $M = 5$ and $\alpha \simeq 0$. Inset in (d): Dissipation pattern $\tilde{a}^{2M}$.

It is also convenient to fix their values as $b_{L,s}^2 = b_L^2[1 + \sqrt{1 - C_L^2}]/2$ and $b_{L,-s}^2 = b_L^2[1 - \sqrt{1 - C_L^2}]/2$, with $0 \leqslant C_L \leqslant 1$, yielding the circularly symmetric case $b_L J_s(\rho)e^{is\varphi}$ for $C_L = 0$ ($b_{L,s} = b_L$, $b_{L,-s} = 0$). The choice $C_L > 0$ ($b_{L,s} > b_{L-s}$) introduces an azimuthal modulation of period π/s and depth C_L in the intensity pattern, but it continues to have a vortex of charge s in the origin. In the limit case with $C_L = 1$ ($b_{L,s} = b_{L,-s}$), the intensity vanishes at $2s$ azimuthal directions.

Two examples of these input beams with respective low and high azimuthal modulation depths ($C_L = 0.3$ and $C_L = 0.98$) are shown in Figs. 6(a)–6(c) and 7(a)–7(c) for $s = 2$. With increasing C_L, the azimuthal total change of the phase in $2\pi s$ about the vortex approaches a steplike variation, reaching $2s$ discontinuous jumps of π in the limit $C_L = 1$, the intensity current $\mathbf{j} = (s/\rho)(b_{L,s}^2 - b_{L,-s}^2)J_s^2(\rho)\mathbf{u}_\varphi$ is always purely azimuthal but increasingly weaker, and
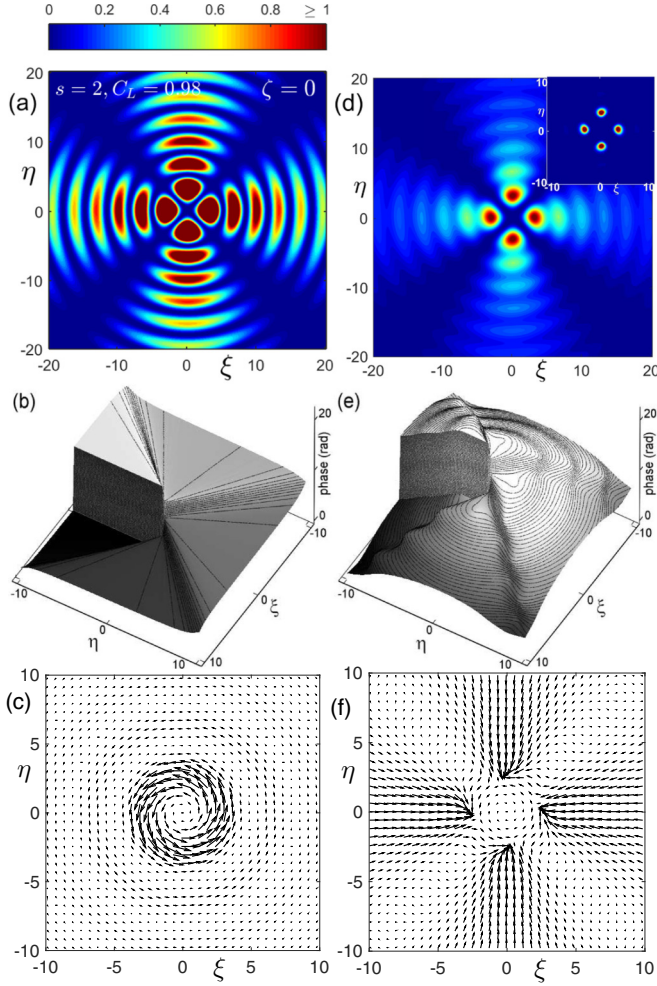
FIG. 7. (a) Intensity, (b) phase, and (c) intensity current of the initial superposition of two Bessel beams of opposite charges, $s = 2$ and $-s = -2$, average amplitude $b_L = 3$, and azimuthal contrast $C_L = 0.98$ ($b_{L,s} = 2.323$ and $b_{L,-s} = 1.899$). (d) Intensity, (e) phase, and (f) intensity current of the final stationary state in the form of a dissipaton formed in a medium with $M = 5$ and $\alpha \simeq 0$. Inset in (d): Dissipation pattern $\tilde{a}^{2M}$.

the associated angular momentum density $L = \tilde{a}^2 \partial\Phi/\partial\varphi = \text{Im}\{\tilde{A}^\star \partial\tilde{A}/\partial\varphi\} = s(b_{L,s}^2 - b_{L,-s}^2)J_s^2(\rho)$ diminishes, vanishing in the limit $C_L = 1$. We focus on these linear Bessel superpositions as input beams because the formed dissipatons share with them a number of their properties, but we stress that the same dissipatons are formed from other beams that do not have any of these properties around the beam center but have equivalent asymptotic inward currents, that is, from $\tilde{A}(\rho,\varphi,0) = b_{L,s}H_s^{(2)}(\rho)e^{is\varphi} + b_{L,-s}H_{-s}^{(2)}(\rho)e^{-is\varphi} + f(\rho,\varphi)$, where $f(\rho,\varphi)$ does not carry any additional inward radial current at a large radius. There may not even be light in the central region of the input beam.

The intensity, phase, and current patterns of the respective dissipatons formed after a transient propagation stage are depicted in Figs. 6(d)–6(f) and Figs. 7(d)–7(f). The corresponding dissipation patterns, with four localized dissipative spots forming a square, are shown in the insets in Figs. 6(d) and 7(d). The dissipatons always preserve the $2s$-fold rotational

symmetry of the input Bessel-beam superposition, a vortex of the same charge s at $\rho = 0$, and an azimuthal modulation of the intensity profile of a depth similar to that of the input beam. We stress that symmetrization into a circularly symmetric nonlinear BVB is never observed, irrespective of the smallness of the C_L of the input beam. As shown below, this is a consequence of the conservation of the inward Hänkel amplitudes. The steplike azimuthal variation of the phase profiles also preserves approximately the same sharpness as that of the input beam, although it changes slightly with the radial distance ρ. In the limit of an input beam with $C_L = 1$, the formed dissipaton continues to have $2s$ null directions, and the azimuthal variation of the phase retains the $2s$ discontinuous jumps. In all cases, a substantial difference from the input beam is that the azimuthal variation of the phase is accompanied by a pronounced radial variation, associated with the permanently converging wave fronts and the permanent radial inward component of the intensity current sustaining the stationarity. For increasing azimuthal input contrast, the radial inward component is accompanied by a decreasing azimuthal component and angular momentum, which vanish in the limit $C_L = 1$.

In the above examples, we chose $\alpha \simeq 0$ for simplicity, but similar properties hold for $0 \leqslant \alpha \leqslant \alpha_{\text{max}}$, where α_{max} depends now on s, b_L, C_L, and M. For $\pm s = \pm 1$ and $\pm s = \pm 3$, the intensity patterns of dissipatons with twofold and sixfold rotational symmetry formed in a medium with $M = 5$ and cone angles and Kerr nonlinearities such that $\alpha \simeq 0$ and α_{max} are depicted in Fig. 8. The insets show the corresponding two-spot and six-spot dissipation patterns. We note that even if the intensity profile is weakly localized and becomes increasingly irregular with increasing α, the dissipation patterns continue to be extremely localized and ordered.

Asymptotic radial and azimuthal structure of dissipatons with $2s$-fold rotational symmetry

The above structure of these dissipatons is reflected in the structure beyond the dissipative region, which admits a more detailed analytical description than for general dissipatons. The asymptotic form in Eq. (13) for these dissipatons reads

$$\tilde{A} \simeq \frac{1}{2}\Big\{\big[b_{\text{out},s}H_s^{(1)}(\rho) + b_{\text{in},s}H_s^{(2)}(\rho)\big]e^{is\varphi} + \big[b_{\text{out},-s}H_{-s}^{(1)}(\rho) + b_{\text{in},-s}H_{-s}^{(2)}(\rho)\big]e^{-is\varphi}\Big\}e^{-i\zeta}. \quad (24)$$

Equivalently, Eq. (14) also holds, where now

$$b_{\text{out}}(\varphi) = b_{\text{out},s}e^{is(\varphi - \frac{\pi}{2})} + b_{\text{out},-s}e^{-is(\varphi - \frac{\pi}{2})}, \quad (25)$$

$$b_{\text{in}}(\varphi) = b_{\text{in},s}e^{is(\varphi + \frac{\pi}{2})} + b_{\text{in},-s}e^{-is(\varphi + \frac{\pi}{2})} \quad (26)$$

represent harmonic azimuthal oscillations of period $2\pi/s$. Consequently, the contrast $C(\varphi)$ of the radial oscillations in the intensity profile along each azimuthal angle φ and its average value $R(\varphi)$ repeat themselves each period π/s, as expected. For the dissipatons in Figs. 6 and 7, Figs. 9(a) and 9(b) and 10(a) and 10(b) depict their intensity profiles and their asymptotic forms satisfying the conservation of the inward Hänkel amplitudes, $|b_{\text{in},s}| = b_{L,s}$, $|b_{\text{in},-s}| = b_{L,-s}$, and the replenishment condition, $|b_{\text{in},s}|^2 + |b_{\text{in},-s}|^2 - |b_{\text{out},s}|^2 - |b_{\text{out},-s}|^2 = N_\infty$. From these values, the contrasts of the radial
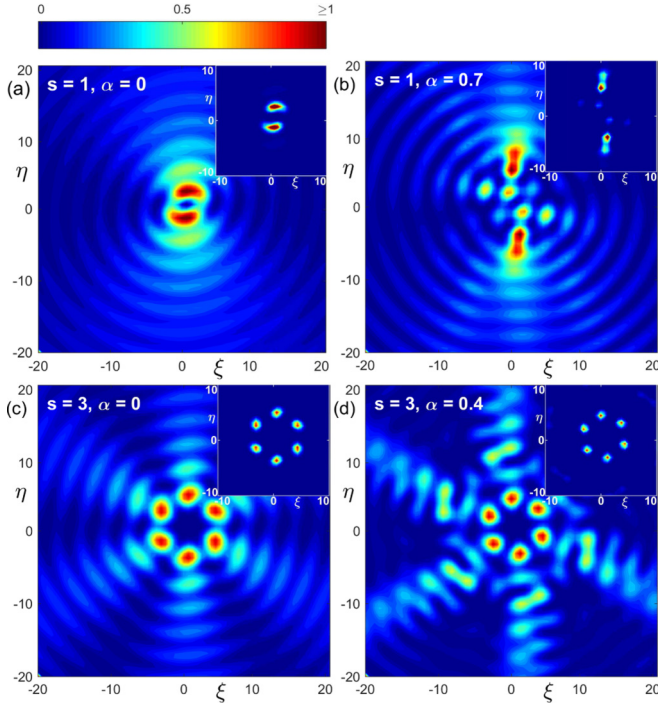
FIG. 8. (a, b) Intensity and dissipation patterns (insets) of the dissipatons formed starting from two conical beam superpositions with average amplitude $b_L = 3$, contrast $C = 0.8$ ($b_{L,s} = 2.683$ and $b_{L,-s} = 1.342$), and $s = 1$ in media with $M = 5$ and cone angles and Kerr nonlinearity such that $\alpha \simeq 0$ and $\alpha = \alpha_{max}$. (c, d) The same, except that $s = 3$.

oscillations in each azimuthal direction, $C(\varphi)$, are evaluated from Eqs. (25) and (18) and are plotted as solid gray curves in Figs. 9(c) and 10(c). As for nonlinear BVBs, dissipation manifests in a loss of radial oscillation contrast (from unity for the input beam), with the peculiarity that the decrease depends on the azimuthal direction and is more pronounced along the directions with a higher intensity (e. g., at $\varphi = 0$).

For dissipatons with $2s$-fold rotational symmetry, using the asymptotic forms of the Hänkel functions in Eq. (12) again, but now grouping the terms with the same azimuthal dependence, Eq. (24) can alternatively be written as

$$\tilde{A} = \frac{1}{\sqrt{2\pi\rho}}[b_s(\rho)e^{is\varphi} + b_{-s}(\rho)e^{-is\varphi}]e^{-i\zeta}, \quad (27)$$

where we have defined

$$b_s(\rho) = b_{out,s}e^{i(\rho - \frac{\pi}{4} - \frac{\pi s}{2})} + b_{in,s}e^{-i(\rho - \frac{\pi}{4} - \frac{\pi s}{2})}, \quad (28)$$

$$b_{-s}(\rho) = b_{out,-s}e^{i(\rho - \frac{\pi}{4} + \frac{\pi s}{2})} + b_{in,-s}e^{-i(\rho - \frac{\pi}{4} + \frac{\pi s}{2})}. \quad (29)$$

In this form, the intensity profile at a large radius is also given by

$$2\pi\rho|\tilde{A}|^2 \simeq |b_s(\rho)|^2 + |b_{-s}(\rho)|^2 + 2|b_s(\rho)||b_{-s}(\rho)|$$
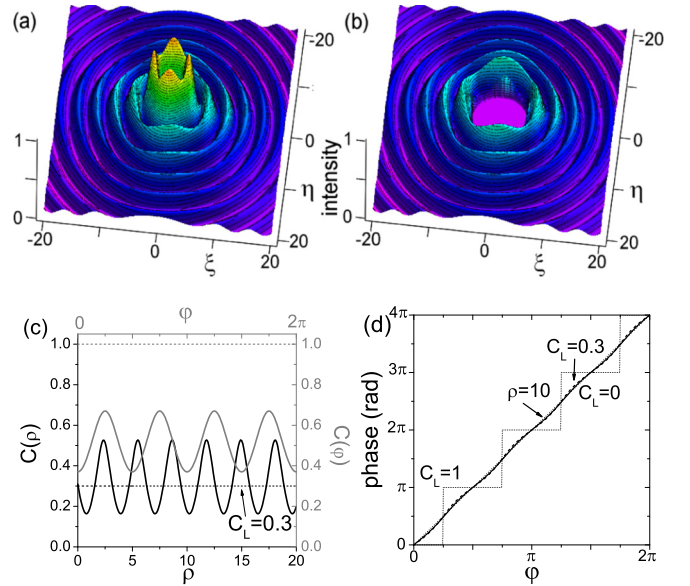$$\times \cos[2s\varphi + \arg b_s(\rho) - \arg b_{-s}(\rho)]. \quad (30)$$

FIG. 9. (a, b) The intensity profile and its asymptotic form from Eq. (24) (for $\rho > 5$) of the dissipaton in Fig. 6 formed from the input Bessel-beam superposition with $s = 2$ and $-s = -2$, $b_L = 3$, and $C_L = 0.3$. For the asymptotic form in Eq. (24), $b_{in,s} = b_{L,s} = 2.965$, $b_{in,-s} = b_{L,-s} = 0.455$, $b_{out,s} = 0.811$, $b_{out,-s} = -0.153$, satisfying $|b_{in,s}|^2 + |b_{in,-s}|^2 - |b_{out,s}|^2 - |b_{out,-s}|^2 = N_\infty = 8.34$. (c) Dashed and solid gray curves: Contrast of the radial oscillations in each azimuthal direction, evaluated from the above Hänkel amplitudes and Eqs. (25) and (18) for the input Bessel-beam superposition and for the dissipaton. Dashed and solid black curves: Contrast of the azimuthal oscillations at each radius, obtained from the Hänkel amplitudes and Eqs. (28) and (31) for the input Bessel-beam superposition (equal to $C_L = 0.3$) and for the dissipaton. (d) Azimuthal variation of the phase at the indicated radius, obtained from the Hänkel amplitudes, and Eqs. (28) and (34). The dashed curve represents the same quantity for the input beam with $C_L = 0.3$, and dotted curves the azimuthal variation of the phase in the limit cases of input beams with $C_L = 0$ and $C_L = 1$, in which case the discontinuous jumps of the phase are preserved.

As a function of φ, these are harmonic oscillations of period π/s of ρ-dependent contrast

$$C(\rho) = \frac{2|b_s(\rho)||b_{-s}(\rho)|}{|b_s(\rho)|^2 + |b_{-s}(\rho)|^2} \quad (31)$$

about a ρ-dependent average value $R(\rho) = |b_s(\rho)|^2 + |b_{-s}(\rho)|^2$. The azimuthal contrast as a function of the radial distance for dissipatons in Figs. 9(a) and 10(a) are plotted as black curves in Figs. 9(c) and 10(c). As shown, the azimuthal contrast, which was independent of ρ and equal to C_L for the input Bessel-beam superposition, oscillates with the radial distance, remaining, however, of the same order as for the input beam, C_L, as observed from the numerical simulations. In the particular dissipatons formed from $C_L = 1$ ($b_{L,s} = b_{-L,s} = b_L/\sqrt{2}$), symmetry considerations ($b_{in,s} = b_{in,-s}$ and $b_{,out,s} = b_{out,-s}$) imply that $b_{-s}(\rho) = (-1)^s b_s(\rho)$, and therefore $C(\rho) = 1$ too; i.e., the dissipaton preserves the $2s$ directions of zero intensity of the input Bessel-beam superposition, as described from the numerical simulations.
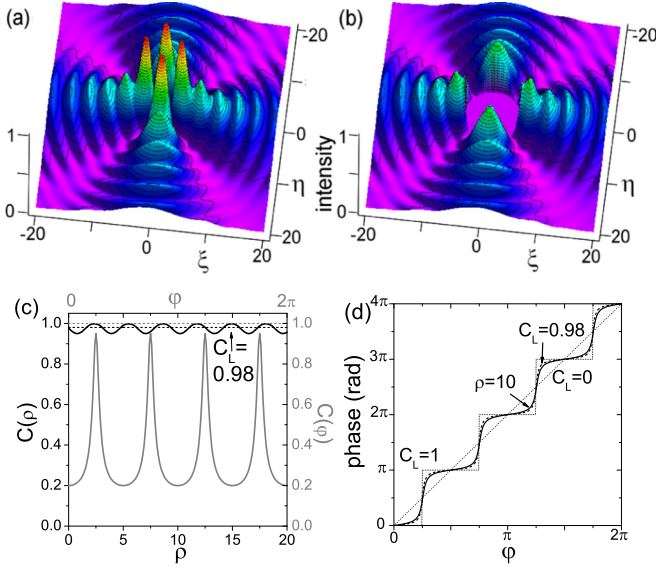
FIG. 10. (a, b) Intensity profile and its asymptotic form from Eq. (24) (for $\rho > 5$) of the dissipaton in Fig. 7 formed from the input Bessel-beam superposition with $s = 2$ and $-s = -2$, $b_L = 3$, and $C_L = 0.98$. For the asymptotic form in Eq. (24), $b_{in,s} = b_{L,s} = 2.323$, $b_{in,-s} = b_{L,-s} = 1.899$, $b_{out,s} = 0.367$, $b_{out,-s} = 0.057$, satisfying $|b_{in,s}|^2 + |b_{in,-s}|^2 - |b_{out,s}|^2 - |b_{out,-s}|^2 = N_\infty = 8.76$. (c) Dashed and solid gray curves: Contrast of the radial oscillations in each azimuthal direction, evaluated from the above Hänkel amplitudes and Eqs. (25) and (18) for the input Bessel-beam superposition and for the dissipaton. Dashed and solid black curves: Contrast of the azimuthal oscillations at each radius, obtained from the Hänkel amplitudes and Eqs. (28) and (31) for the input Bessel-beam superposition (equal to $C_L = 0.98$) and for the dissipaton. (d) Azimuthal variation of the phase at the indicated radius, obtained from the Hänkel amplitudes and Eqs. (28) and (34). The dashed curve represents the same quantity for the input beam with $C_L = 0.98$. Dotted curves are as in Fig. 9.

In addition to the inward radial component of the intensity flux, these dissipatons with $2s$-fold symmetry carry the azimuthal component $j_\varphi \simeq (s/2\pi\rho)[|b_s(\rho)|^2 - |b_{-s}(\rho)|^2]/\rho$ at a large radius. Interestingly, while the intensity and phase profiles exhibit pronounced azimuthal variations, the azimuthal flux remains circularly symmetric. Thus, the vector expression of the intensity current is

$$\mathbf{j} \simeq \frac{[|b_{out}(\varphi)|^2 - |b_{in}(\varphi)|^2]}{2\pi\rho}\mathbf{u}_\rho + \frac{s}{\rho}\frac{[|b_s(\rho)|^2 - |b_{-s}(\rho)|^2]}{2\pi\rho}\mathbf{u}_\varphi. \tag{32}$$

Accordingly, the angular momentum density is given by

$$L = \mathrm{Im}\left\{\tilde{A}^\star \frac{\partial \tilde{A}}{\partial \varphi}\right\} \simeq \frac{s}{2\pi\rho}[|b_s(\rho)|^2 - |b_{-s}(\rho)|^2] \tag{33}$$

and is also circularly symmetric. These properties are also of interest in order to evaluate the azimuthal derivative of the phase as $\partial\Phi/\partial\varphi = L/|\tilde{A}|^2$. Upon integration with the above asymptotic expressions of L and $|\tilde{A}|^2$, the phase is asymptotically given by

$$\Phi \simeq \tan^{-1}\left\{\frac{|b_s(\rho)| - |b_{-s}(\rho)|}{|b_s(\rho)| + |b_{-s}(\rho)|}\tan[s\varphi + \kappa(\rho)]\right\}, \tag{34}$$

with $\kappa(\rho) = [\arg b_s(\rho) - \arg b_{-s}(\rho)]/2$ (the term $-\zeta$ on propagation is omitted). From Eqs. (28) and (31), the above relation can also be expressed as

$$\Phi \simeq \tan^{-1}\left\{\sqrt{\frac{1 - C(\rho)}{1 + C(\rho)}}\tan[s\varphi + \kappa(\rho)]\right\}, \tag{35}$$

relating the azimuthal variation of the phase to that of the intensity. The azimuthal phase variation of the dissipatons in Figs. 9(a) and 10(a) are plotted in Figs. 9(d) and 10(d), respectively, at a particular radius. These explain the increasing sharpness of the azimuthal phase variation with increasing azimuthal contrast of the intensity $C(\rho)$ and the fact that in the limit $C(\rho) = 1$ (obtained from $C_L = 1$), the phase of the azimuthons continues to display $2s$ discontinuous π jumps of the input Bessel-beam superposition.

Dissipatons with $2s$-fold rotational symmetry share with azimuthons, and their limiting cases of vortex solitons and soliton clusters, similar azimuthal modulation of the intensity patterns and similar stairlike azimuthal variation of the phase [8,9], but as pointed out in Sec. I, they are supported by completely different mechanisms. Also, azimuthons are generally rotating, and the number of azimuthal maxima and vortex charge at their center are independent properties, while these dissipatons are static, and the number of maxima is $2s$ if the charge is s.

VI. CONCLUSIONS

In conclusion, we have described a broad family of propagation-invariant and robust conical beams in media with Kerr-type nonlinearities and nonlinear absorption, with the property of continuously dissipating power along narrow and ordered channels, whose number and geometrical disposition can be easily controlled. We have described their spatial structure semianalytically and found the laws that govern their formation from superpositions of Bessel beams. The structure of the power reservoir that supports the stationarity is described by a superposition of unbalanced Bessel beams preserving the cone angle, topological charges, and inward Hänkel amplitudes of each of the input Bessel beams forming the superposition, and with outward Hänkel-beam amplitudes such that the net inward power flux replenishes the nonlinear power losses.

We have limited our considerations to "ideal" dissipatons with an unlimited amount of power in their reservoir formed from similar ideal Bessel beams or equivalent inward intensity currents. In real settings, Bessel beams are formed only up to a maximum radial distance, say r_{max}, and therefore the reservoir is of limited capacity. As previously described for other conical beams [26,35,40,41], the reservoir will be depleted and the dissipaton will therefore decay, at a distance of the order of the diffraction-free distance $z_{free} \simeq r_{max}/\theta$ (or $\zeta_{free} \simeq \rho_{max}/2$ with our dimensionless axial and radial distances).

In filamentation experiments, the new degrees of control offered by these beams with regard to the number and disposition of plasma channels may open new possibilities in short-range applications such as material laser ablation and waveguide writing and in long-range applications such as filamentation guiding of weak waves in the atmosphere [42–46]. Also for

these applications, it may also be of interest to investigate the existence of dissipative general azimuthons having, like azimuthons in conservative models, intensity patterns with an independent number of azimuthal maxima and vortex charge at their center and rotating at arbitrary angular velocities.

[1] B. A. Malomed, D. Mihalache, F. Wise, and L. Torner, Spatiotemporal optical solitons, J. Opt. B **7**, R53 (2005).

[2] Y. S. Kivshar and G. P. Agrawal, *Optical Solitons: From Fibers to Photonic Crystals* (Academic Press, San Diego, CA, 2003).

[3] Z. Chen, M. Segev, and D. N Christodoulides, Optical spatial solitons: Historical overview and recent advances, Rep. Prog. Phys. **75**, 086401 (2012).

[4] N. Akhmediev and A. Ankiewicz (eds.) *Dissipative Solitons*. Lecture Notes in Physics 661 (Springer-Verlag, Berlin, 2005).

[5] T. Ackemann, W. J. Firth, and G.-L. Oppo, Fundamentals and applications of spatial dissipative solitons in photonic devices, Adv. At. Mol. Opt. Phys. **57**, 323 (2009).

[6] B. A. Malomed, Spatial solitons supported by localized gain, J. Opt. Soc. Am. B **31**, 2460 (2014).

[7] V. I. Kruglov and R. A. Vlasov, Spiral self-trapping propagation of optical beams in media with cubic nonlinearity, Phys. Lett. A **111**, 401 (1985).

[8] A. S. Desyatnikov, A. A. Sukhorukov, and Yu. S. Kivshar, Azimuthons: Spatially Modulated Vortex Solitons, Phys. Rev. Lett. **95**, 203904 (2005).

[9] A. Minovich, D. N. Neshev, A. S. Desyatnikov, W. Krolikowski, and Y. S. Kivshar, Observation of optical azimuthons, Opt. Express **17**, 23610 (2009).

[10] A. S. Desyatnikov and Yu. S. Kivshar, Rotating Optical Soliton Clusters, Phys. Rev. Lett. **88**, 053901 (2002).

[11] A. S. Desyatnikov, L. Torner, and Y. S. Kivshar, Optical vortices and vortex solitons, Prog. Opt. **47**, 291 (2005).

[12] P. V. Paulau, D. Gomila, P. Colet, N. A. Loiko, N. N. Rosanov, T. Ackemann, and W. J. Firth, Vortex solitons in lasers with feedback, J. Opt. Express **18**, 8859 (2010).

[13] L. C. Crasovan, B. A. Malomed, and D. Mihalache, Stable vortex solitons in the two-dimensional Ginzburg-Landau equation, Phys. Rev. E **63**, 016605 (2000).

[14] Y. Zhang, M. Belic, Z. Wu, C. Yuan, R. Wang, K. Lu, and Y. Zhang, Multicharged optical vortices induced in a dissipative atomic vapor system, Phys. Rev. A **88**, 013847 (2013).

[15] M. A. Porras, A. Parola, D. Faccio, A. Dubietis, and P. Di Trapani, Nonlinear Unbalanced Bessel Beams: Stationary Conical Waves Supported by Nonlinear Losses, Phys. Rev. Lett. **93**, 153902 (2004).

[16] A. Couairon and A. Mysyrowicz, Femtosecond filamentation in transparent media, Phys. Rep. **441**, 47 (2007).

[17] L. Bergé, S. Skupin, R. Nuter, J. Kasparian, and J. P. Wolf, Ultrashort filaments of light in weakly ionized, optically transparent media, Rep. Prog. Phys. **70**, 1633 (2007).

[18] L. Bergé and S. Skupin, Modeling ultrashort filaments of light, Discr. Cont. Dynam. Syst. **23**, 1099 (2009).

[19] A. Dubietis, E. Kucinskas, G. Tamosauskas, E. Gaizauskas, M. A. Porras, and P. Di Trapani, Self-reconstruction of light filaments, Opt. Lett. **29**, 2893 (2004).

[20] E. Gaizauskas, A. Dubietis, V. Kudriasov, V. Sirutkaitis, A. Couairon, D. Faccio, and P. Di Trapani, On the role of conical waves in self-focusing and filamentation of femtosecond pulses with nonlinear losses, Top. Appl. Phys. **114**, 457 (2009).

[21] D. Faccio, M. A. Porras, A. Dubietis, G. Tamosauskas, E. Kucinskas, A. Couairon, and P. Di Trapani, Angular and chromatic dispersion in Kerr-driven conical emission, Opt. Commun. **265**, 672 (2006).

[22] L. Roso, J. San Román, I. J. Sola, C. Ruiz, V. Collados, J. A. Pérez, C. Méndez, J. R. Vázquez de Aldana, I. Arias, and L. Plaja, Propagation of terawatt laser pulses in the air, Appl. Phys. A **92**, 865 (2008).

[23] A. A. Zemlyanov and A. D. Bulygin, Features of the development of light field perturbations in a Kerr medium with nonliner absorption, Atmos. Ocean. Opt. **26**, 85 (2013).

[24] A. Dubietis, G. Valiulis, and A. Varanavicius, Nonlinear localization of light, Lith. J. Phys. **146**, 7 (2006).

[25] D. Faccio, A. Matijosius, A. Dubietis, R. Piskarskas, A. Varanavičius, E. Gaizauskas, A. Piskarskas, A. Couairon, and P. Di Trapani, Near- and far-field evolution of laser pulse filaments in Kerr media, Phys. Rev. E **72**, 037601 (2005).

[26] J. Durnin, J. J. Miceli, and J. H. Eberly, Diffraction-Free Beams, Phys. Rev. Lett. **58**, 1499 (1987).

[27] G. A. Siviloglou, J. Broky, A. Dogariu, and D. N. Christodoulides, Observation of Accelerating Airy Beams, Phys. Rev. Lett. **99**, 213901 (2007).

[28] M. A. Porras and C. Ruiz-Jiménez, Nondiffracting and nonattenuating vortex light beams in media with nonlinear absorption of orbital angular momentum, J. Opt. Soc. Am B **31**, 2657 (2014).

[29] V. Jukna, C. Milián, C. Xie, T. Itina, J. Dudley, F. Courvoisier, and A. Couairon, Filamentation with nonlinear Bessel vortices, Opt. Express **22**, 25410 (2014).

[30] C. Xie, V. Jukna, C. Milián, R. Giust, I. Ouadghiri-Idrissi, T. Itina, J. M. Dudley, A. Couairon, and F. Courvoisier, Tubular filamentation for laser material processing, Sci. Rep. **5**, 8914 (2015).

[31] A. Lotti, D. Faccio, A. Couairon, D. G. Papazoglou, P. Panagiotopoulos, D. Abdollahpour, and S. Tzortzakis, Stationary nonlinear Airy beams, Phys. Rev. A **84**, 021807(R) (2011).

[32] P. Polesana, M. Franco, A. Couairon, D. Faccio, and P. Di Trapani, Filamentation in Kerr media from pulsed Bessel beams, Phys. Rev. A **77**, 043814 (2008).

[33] S. Akturk, B. Zhou, M. Franco, A. Couairon, A. Mysyrowicz, Generation of long plasma channels in air by focusing ultrashort laser pulses with an axicon, Opt. Commun. **282**, 129 (2009).

[34] P. Polesana, A. Dubietis, M. A. Porras, E. Kucinskas, D. Faccio, A. Couairon, and P. Di Trapani, Near-field dynamics of ultrashort pulsed Bessel beams in media with Kerr nonlinearity, Phys. Rev. E **73**, 056612 (2006).

[35] P. Polesana, A. Couairon, D. Faccio, A. Parola, M. A. Porras, A. Dubietis, A. Piskarskas, and P. Di Trapani, Observation of Conical Waves in Focusing, Dispersive, and Dissipative Kerr Media, Phys. Rev. Lett. **99**, 223902 (2007).

[36] P. Polesana, D. Faccio, P. Di Trapani, A. Dubietis, A. Piskarskas, A. Couairon, and M. A. Porras, High localization, focal depth and contrast by means of nonlinear Bessel beams, Opt. Express **13**, 6160 (2005).

[37] D. Majus and A. Dubietis, Statistical properties of ultrafast supercontinuum generated by femtosecond Gaussian and Bessel beams: A comparative study, J. Opt. Soc. Am. B **30**, 994 (2013).

[38] S. Akturk, B. Zhou, A. Houard, M. Franco, A. Couairon, and A. Mysyrowicz, Long plasma channels formed by axicon-focused filaments, Proc. SPIE **7027**, 70271E (2008).

[39] G. Kaya, N. Kaya, M. Sayrac, Y. Boran, J. Strohaber, A. A. Kolomenskii, M. Amani, and H. A. Schuessler, Extension of filament propagation in water with Bessel-Gaussian beams, AIP Adv. **6**, 035001 (2016).

[40] M. A. Porras, C. Ruiz-Jiménez, and J. C. Losada, Underlying conservation and stability laws in nonlinear propagation of axicon-generated Bessel beams, Phys. Rev. A **92**, 063826 (2015).

[41] M. A. Porras, Márcio Carvalho, Hervé Leblond, and Boris A. Malomed, Stabilization of vortex beams in Kerr media by nonlinear absorption, Phys. Rev. A **94**, 053810 (2016).

[42] F. Courvoisier, J. Zhang, K. Bhuyan, M. Jacquot and J. M. Dudley, Applications of femtosecond Bessel beams to laser ablation, Appl. Phys. A **112**, 29 (2013).

[43] M. K. Bhuyan, P. K. Velpula, J. P. Colombier, T. Olivier, N. Faure, and R. Stoian, Single-shot high aspect ratio bulk nanostructuring of fused silica using chirp-controlled ultrafast laser Bessel beams, Appl. Phys. Lett. **104**, 021107 (2014).

[44] G. Krishna Podagatlapalli, S. Hamad, Md. Ahamad Mohiddon, and S. Venugopal Rao, Fabrication of nanoparticles and nanostructures using ultrafast laser ablation of silver with Bessel beams, Laser Phys. Lett. **12**, 036003 (2015).

[45] C. L. Arnold, S. Akturk, A. Mysyrowicz, V. Jukna, A. Couairon, T. Itina, R. Stoian, C. Xie, J. M. Dudley, and F. Courvoisier, Nonlinear Bessel vortex beams for applications, J. Phys. B: At. Mol. Opt. Phys. **48**, 094006 (2015).

[46] F. Courvoisier, R. Stoian, and A. Couairon, Ultrafast laser micro- and nano-processing with nondiffracting and curved beams, Opt. Laser Technol. **80**, 125 (2016).

[47] L. Froehly, M. Jacquot, P. A. Lacourt, J. M. Dudley, and F. Courvoisier, Spatiotemporal structure of femtosecond Bessel beams from spatial light modulators, J. Opt. Soc. Am. A **31**, 790 (2014).

[48] T. W. Clark, R. F. Offer, S. Franke-Arnold, A. S. Arnold, and N. Radwell, Comparison of beam generation techniques using a phase only spatial light modulator, Opt. Express **24**, 6249 (2016).

[49] R. Vasilyeu, A. Dudley, N. Khilo, and A. Forbes, Generating superpositions of higher order Bessel beams, Opt. Express **17**, 23389 (2009).

[50] J. Arlt and K. Dholakia, Generation of high-order Bessel beams by use of an axicon, Opt. Commun. **177**, 297 (2000).

[51] A. Couairon, A. Lotti, P. Panagiotopoulos, D. Abdollahpour, D. Faccio, D. G. Papazoglou, S. Tzortzakis, F. Courvoisier, and J. M. Dudley, Ultrashort pulse filamentation with Airy and Bessel beams, Proc. SPIE **8770**, 87701E (2013).